partial transparency of the sample and misalignment of the diffractometer (Cheary & Coelho, 1992). Even if a monochromator is used to select only the $K\alpha_1$ line, the radiation spectrum from an X-ray tube consists of several Lorentzian functions owing to satellite transitions.

Axial divergence produces a pronounced asymmetry of low-angle diffraction peaks to the low-angle direction (and on the high-angle side of peaks with 2θ near 180°). If the incident or diffracted rays are out of the equatorial plane, they will be intercepted at a detector setting below (above) the actual diffraction angle if it is small (close to 180°), respectively. The effect can be minimized, but not completely eliminated, by narrowing the beam-defining apertures in the equatorial direction, or by introduction of parallel-blade Soller (1924) slits. The full treatment of the effect of axial divergence in a Bragg–Brentano diffractometer has been presented in a computationally convenient form (Cheary & Coelho, 1998).

It is generally easier to model the instrumental response function of a powder X-ray diffractometer based on a synchrotron-radiation source with an analyser crystal, because the transfer functions of the various optical elements are simpler to express. One approach is to approximate the wavelength- and angle-dependent reflectivity of monochromator and analyser crystals by Gaussians, and derive a closed-form expression for the width of the instrument response function (Sabine, 1987). This has been extended to include collimating and focusing (in the scattering plane) mirrors (Gozzo *et al.*, 2006); see Chapter 3.1 for a full description of the relevant optical configurations. A shortcoming of this analytical approach is that the correct single-crystal reflectivity function is not a Gaussian, so it cannot account for the correct line shape, only provide an estimate of its width. Numerical convolutions to accurately model the line-shape function have been performed, and produce excellent agreement with measured profiles (Masson *et al.*, 2003).

Instead of the analytical approach described in the previous few paragraphs, one frequently writes a parametrized function for the measured line shape without concern for the connection between the numerical values of the parameters and the microscopic properties of the sample or the geometry of the diffractometer. For example, one can use the Caglioti form for diffraction peak width [equation (3.2.13)] on any diffractometer, and adjust the parameters U, V and W to some measured standard sample. If size and strain contributions to sample-dependent broadening are both regarded as Lorentzians, they could be combined as $\Gamma = X/\cos\theta + Y\tan\theta$. (Here we make use of the fact that the convolution of two Lorentzians is a Lorentzian whose width is the sum of the individual widths. For Gaussians, the widths combine in quadrature, *i.e.*, $\Gamma^2 = \Gamma_1^2 + \Gamma_2^2$.) In the general case, where neither the instrumental response function nor the sample broadening is purely a Gaussian or Lorentzian function, one can write an empirical line shape as the approximate convolution of a Gaussian and a Lorentzian, with widths given by

$$\begin{aligned}\Gamma_G &= (U\tan^2\theta + V\tan\theta + W + P/\cos^2\theta)^{1/2},\\ \Gamma_L &= X/\cos\theta + Y\tan\theta.\end{aligned} \tag{3.2.14}$$

This is one of the flexible line-shape models available in the widely used program *GSAS* (Larson & Von Dreele, 2004). It is still possible to make a semi-quantitative statement about sample properties by comparing refined parameters against a standard sample; for example, size broadening will increase the P and X parameters, and strain will increase U and Y. A similar model is used in the *FullProf* software (Rodríguez-Carvajal, 1993, 2001; Kaduk & Reid, 2011).

3.2.3. Complications due to non-ideal sample or instrument properties

In this section, we consider various factors that modify powder X-ray diffraction data relative to the idealized situation described above.

3.2.3.1. *Absorption within a homogeneous sample*

In equations (3.2.2) and (3.2.10), it was assumed that the neither the incident nor the diffracted radiation is absorbed within the sample. However, it is generally the case that neutrons or X-rays are attenuated as they travel through any material, such that the fraction of original intensity surviving after a distance x is $I(x)/I(0) = \exp(-\mu x)$. Here μ is the linear absorption coefficient, which generally depends strongly on the composition of the sample and the X-ray wavelength.

X-ray attenuation coefficients for elements are often given as mass attenuation coefficients, μ/ρ, in units of cm^2 g^{-1}. These are available in various sources, such as *International Tables for Crystallography*, Volume C, Table 4.2.4.3, or from internet resources such as http://11bm.xray.aps.anl.gov/absorb/absorb.php. The exact positions of X-ray absorption edges can depend on the chemical environment of the atom, and so tabulated or computed atomic absorption coefficients are not entirely trustworthy within about ±100 eV of an absorption edge. The X-ray mass attenuation coefficient is related to the imaginary part of the atomic scattering factor [equation (3.2.6)] as $\mu_m = 2r_e\lambda f''/m$, where m is the atomic mass. For a compound or other mixture of elements of total density ρ in which the (dimensionless) mass fraction of element i is g_m^i, the X-ray linear absorption constant is given by

$$\mu_{\text{X-ray}} = \rho\sum_i g_m^i(\mu_m/\rho)^i.$$

In the case of neutrons used for powder diffraction, the absorption cross section is typically tabulated in barns (1 barn = 10^{-24} cm^2); see Table 4.4.4.1 in *International Tables for Crystallography*, Volume C or websites such as http://www.ncnr.nist.gov/resources/n-lengths/list.html. The neutron absorption cross section is generally inversely proportional to velocity, and values are usually tabulated for neutrons with a speed of 2200 m s^{-1} (*i.e.*, 25.3 meV kinetic energy, 1.80 Å wavelength). For neutrons, the equivalent expression with absorption cross sections depends on the number densities g_n^i (atoms/volume) of each element:

$$\mu_{\text{neutron}} = \sum_i g_n^i(\sigma_{\text{abs}}^i + \sigma_{\text{inc}}^i).$$

Considering absorption, the effective volume is given by an integral over the sample,

$$V_{\text{eff}} = \int \mathrm{d}^3\,\mathbf{R}\exp[-\mu(L_{\text{in}} + L_{\text{out}})], \tag{3.2.15}$$

where L_{in} and L_{out} are the paths of the incident and diffracted radiation to the point $\mathbf{R}$ within the sample, respectively.

The simplest case is of a sample in the form of a flat plate, with a thickness significantly greater than $1/\mu$, in the dividing position so that the angles of incidence and diffraction from the plane of the sample are both equal to θ. Let the dimensions of the beam be W in the equatorial direction (in the diffraction plane) and H in the axial direction (parallel to the diffractometer axis, *i.e.*, perpendicular to the scattering plane) as shown in Fig. 3.2.2.

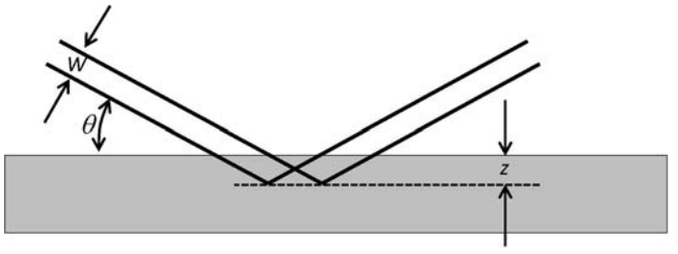

Figure 3.2.2
Sketch illustrating symmetrical diffraction from a flat sample.

Assume that the detector is large enough in the equatorial direction that all diffracted radiation is captured (*i.e.*, no loss of signal due to parallax). Radiation scattered from a volume element a distance z below the surface of the sample will have a total path length $2z/\sin\theta$; integration yields an effective sample volume of $WH/2\mu$, independent of diffraction angle. The situation is more complicated if a flat sample is not optically deep or if the sample is shorter than $W/\sin\theta$; in either case, computation of the effective volume is straightforward, as long as the sample geometry is known with sufficient accuracy. The calculations are described in detail in Chapter 5.4 of this volume.

Another important case is that of a cylindrical sample, such as a Lindemann capillary for X-rays or a can of appropriate material (often vanadium) for neutrons. The integration for $V_{\rm eff}$ above is given in convenient form for computation by Ida (2010), and is tabulated in *International Tables for Crystallography*, Volume C, Section 6.3.3.2. In the case of monochromatic radiation (neutrons or X-rays), for a given absorption constant μ, $V_{\rm eff}$ is an increasing function of diffraction angle 2θ so that higher-angle peaks will appear relatively stronger. Weak-to-moderate absorption from a cylindrical sample affects the observed intensities in essentially the same algebraic form as a negative effective Debye–Waller factor (Hewat, 1979), leading to significantly underestimated (perhaps even negative) measured Debye–Waller factors. In the case of pulsed neutrons, the effect is compounded by the fact that the absorption cross section is generally inversely proportional to the neutron velocity; consequently, in a given detector, faster neutrons, representing larger $|\mathbf{G}|$, will suffer less attenuation in the sample.

3.2.3.2. *Absorption with multiphase samples*

One important application of powder diffraction is the quantitative analysis of mixtures. Quantitative phase analysis is covered in detail in Chapter 3.9 of this volume; here we set the stage. If a sample is a mixture of several phases, the powder-diffraction pattern will be the sum of the patterns of each phase, weighted by the fraction of the illuminated volume occupied by that phase. The most common configuration for quantitative analysis by X-ray diffraction is reflection from an optically deep flat-plate sample. In this case, the integrated intensity of a particular reflection from the jth phase is

$$I_{hkl}(j) = I_0 LP(\theta)\frac{m_{hkl}(j)|A_{hkl}(j)|^2}{V^2(j)}\frac{w_m(j)}{\rho(j)\overline{\mu}}, \qquad (3.2.16)$$

where $V(j)$, $w_m(j)$ and $\rho(j)$ are the unit-cell volumes, mass fraction and density of phase j, respectively. Here I_0 is an overall intensity scale factor, $LP(\theta)$ is the Lorentz and polarization factor common to all phases, and $\bar{\mu} = \sum_j w_m(j)\mu(j)$ is the absorption coefficient of all solid phases in the sample. The summation includes all solid phases, even amorphous materials.

Note that the intensity of peaks from a particular phase is not simply proportional to the fraction of that phase present. For example, if there are two phases A and B, the intensity of A peaks will be proportional to

$$\frac{w_m(A)}{w_m(A)[\mu(A)-\mu(B)]+\mu(B)}.$$

3.2.3.3. *Granularity, microabsorption and surface roughness*

The above discussion of absorption in a powder sample is premised on the assumption that the powder sample is sufficiently fine that the beam traverses a large number of grains, *i.e.*, that $\mu\ell \ll 1$, where μ is the absorption coefficient in the solid material and ℓ is a characteristic linear grain dimension. In that case, the effective linear absorption constant is $\bar{\mu} = \mu\rho_{\rm powder}/\rho_{\rm solid}$, independent of the path that the radiation follows through the sample. However, if $\mu\ell$ is not very small, the simple picture of an average absorption length in the sample breaks down, leading to changes in the diffracted intensity.

There have been several treatments of microabsorption due to porosity and surface roughness. Rather than reviewing the literature, this section summarizes work of Hermann & Ermrich (1987) on a flat sample in the symmetrical reflection geometry discussed above. The single-phase sample is taken to be a collection of random polyhedra of average chord length ℓ with packing fraction α_0. The surface has the same lateral correlation length, but the average packing fraction rises from zero at the surface with characteristic dimension t_s, *i.e.*, $\alpha(z) = \alpha_0[1-\exp(-z/t_s)]$, where z is the distance from the surface into the sample. $t_s = 0$ represents an abrupt termination of the bulk porous material.

Hermann & Ermrich find that the diffracted intensity is reduced from the fine powder limit by a factor of $1 - P_{\rm bulk} - P_{\rm surface}$, where

$$P_{\rm bulk} \simeq 2\mu\ell(1-\alpha_0)^2,$$
$$P_{\rm surface} \simeq \frac{2\mu\alpha_0 t_s}{\sin\theta}\left(1-\frac{t_s}{\ell(1-\alpha_0)\sin\theta}\right).$$

If surface roughness is small, there is no dependence on diffraction angle 2θ, and the only effect is an overall reduction of diffracted intensity. Excess surface roughness ($t_s > 0$), as might be produced by allowing a granular powder to settle against a flat surface, leads to additional diminution of diffracted intensity at low angles. The expression for $P_{\rm surface}$ given above is to leading order in $1/\sin\theta$, and is therefore not valid for small grazing angles of incidence. Note that both the surface and bulk correction factors approach zero as $\mu\ell \to 0$. This analysis is in general agreement with analysis and measurements performed by Suortti (1972).

An additional effect of microabsorption in multi-component powders has been considered by Brindley (1945). The principle is illustrated in Fig. 3.2.3. An X-ray propagating through the sample (depicted by the broken line) suffers absorption according to the weighted average $\bar{\mu}$, but an X-ray diffracted in a grain of phase a has travelled further in that phase than average (solid line). If its path in the diffracting grain is x and the total path through the sample is L, absorption will reduce its intensity by a factor

$$\exp(-\mu_a x)\exp[-\overline{\mu}(L-x)].$$